Journal of Power Sources 255 (2014) 70–75

Contents lists available at ScienceDirect

Journal of Power Sources

journal homepage: www.elsevier.com/locate/jpowsour

Short communication

Electronspun nanofiber network anode for a passive direct methanol fuel cell

Peng Chen [a,b], Huijuan Wu [a,b], Ting Yuan [b], Zhiqing Zou [b,*], Haifeng Zhang [b], Junwei Zheng [a], Hui Yang [b,*]

[a] College of Chemistry, Chemical Engineering and Materials Science, Soochow University, Suzhou 215123, China
[b] Shanghai Advanced Research Institute, Chinese Academy of Sciences, Shanghai 201210, China

HIGHLIGHTS

- A nanofiber network catalytic structure (NNCL) is used in the anode of a DMFC.
- The use of the NNCL leads to a significant increase in catalyst utilization.
- The DMFC with 55% reduced anode catalyst loading exhibits a comparable performance.

ARTICLE INFO

Article history:
Received 30 September 2013
Received in revised form
20 November 2013
Accepted 30 December 2013
Available online 8 January 2014

Keywords:
Nanofiber network
Electrospinning
Catalyst utilization
Membrane electrode assembly
Direct methanol fuel cell

ABSTRACT

A novel membrane electrode assembly (MEA) that utilizes a nanofiber network catalytic layer (NNCL) structure in the anode of a passive direct methanol fuel cell (DMFC) leads to a significant decrease in noble metal catalyst loading of a DMFC. When the PtRu (1:1) loading within the NNCL is 1.0 mg cm^{-2}, the maximum power density of a DMFC is ca. 33.0 ± 1.9 mW cm^{-2}, which is even slightly higher than that with a conventional MEA with a PtRu loading of 2.0 mg cm^{-2}. Electrochemical tests show that such a NNCL exhibits a great increase in catalyst utilization and a decrease in charge-transfer resistance of the anode in comparison with the conventional MEA. The improved performance of the novel MEA is definitely due to the formation of the nanofiber network structure in the anode. This study provides a promising way to decrease the utilization of the noble metal catalysts for the proton exchange membrane fuel cells.

1. Introduction

Passive direct methanol fuel cells (DMFCs) have attracted broad interest as potential power sources for portable applications due to their high energy density, lack of pollution, as well as availability and ease of storage of methanol [1,2]. However, there are several issues that have restricted its practical applications, such as sluggish kinetics of both methanol oxidation and oxygen reduction reactions, high noble metal catalyst loading within the membrane electrode assembly (MEA) of the DMFC [3,4].

Generally, the noble metal loading on each side of an MEA is ca. 3–4 mg cm^{-2}, which is very high for the practical application of the DMFCs. To reduce noble metal loading within the MEA, extensive efforts have been made to develop the highly active catalysts with low noble metal content, such as Pt alloys, Pt-shell with low or non-Pt core, hollow structure catalysts, and even non-Pt catalysts [5–12]. On the other hand, the use of nanostructured materials as the catalysts or catalyst supports could lead to an improvement in both catalytic activity and catalyst utilization. As an example, Kim et al. [13] synthesized bimetallic nanowires (NWs) of PtRu and PtRh. The PtRu and PtRh NWs with an atomic ratio of 1:1 exhibit higher catalytic activity for methanol electrooxidation and better stability than the commercial carbon-supported PtRu nanoparticles. Yang et al. [14] reported that the use of single-walled carbon nanotubes (SWCNTs) as the support for Pt nanoparticles leads to a significantly enhanced catalytic activity for methanol oxidation. Also, graphite nanofibers are employed as a support for Pt nanoparticles [15], the graphite nanofiber supported nanoparticles were less susceptible to CO poisoning than the traditional catalysts, likely due to a specific

* Corresponding authors. Fax: +86 21 20325112.
E-mail addresses: zouzq@sari.ac.cn (Z. Zou), yangh@sari.ac.cn, huiyang65@hotmail.com (H. Yang).

0378-7753/$ – see front matter © 2014 Elsevier B.V. All rights reserved.
http://dx.doi.org/10.1016/j.jpowsour.2013.12.130

crystallographic orientations of metal nanoparticles on the graphite nanofibers.

Another alternative way to decrease the use of noble metal is to improve catalysts' utilization by maximizing the triple-phase reaction boundary (TPRB) of the MEA. As reported, two common methods are used for the fabrication of the MEAs: catalyst-coated on gas diffusion electrode (GDE) [16] and catalyst-coated on membrane (CCM) [17,18]. Although the MEA made by CCM method exhibits a thinner catalyst layer, more efficient mass transport and higher catalyst utilization than that by GDE method, the catalyst loading with CCM method is still high and mass transport needs to be further improved [19–21]. In this regard, recent research focuses have been placed on the fabrication of nanostructured MEAs to maximize the active sites of the TPRB. Marc Michel et al. [22] reported that the use of carbon nanotube and carbon nanofiber composites fabricated by layer-by-layer assembly results in an extensive percolating network, and thus improving the fuel cell's performance. By tuning the size of congeries formed between catalyst nanoparticles and Nafion ionomers within the MEA [23], a significant enhancement in DMFC's performance is obtained, due to an improvement in both catalyst and Nafion utilization. A typical example is that the nanostructured thin film catalyst, developed by Minnesota Mining and Manufacturing (3M) Company, comprises high aspect ratio elongated particles onto oriented crystalline organic whiskers. With such nanostructured thin film catalyst, Pt loading within the MEA could be reduced to 0.12 mg cm^{-2} for an H_2/O_2 fuel cell and with an enhanced fuel cell's performance [24]. Obviously, above results strongly suggest that the construction of nanostructured catalytic layer within the MEA could lead to an improvement in both catalyst utilization and DMFC's performance, thus allowing a decrease in noble metal loading within the MEA.

Electrospinning is a very useful technique that allows the formation of continuous nanofibers with high surface area, remarkable porosity and permeability [25,26]. Based on these advantages, electrospinning has been used to construct separators for Li ions' batteries [27,28], 3-D electrodes for supercapacitors [29,30] and biosensors [31,32], and supports for the catalysts [33,34]. Recently, Pintauro et al. [35] reported the use of electrospun nanofiber mats, composing of Pt/C catalyst and Nafion resin, as the cathode for an H_2/O_2 fuel cell. Although the maximal power density of 524 mW cm^{-2} at 80 °C is lower than that of conventional H_2/O_2 fuel cell with a power density of ca. 750 mW cm^{-2} [36,37], Pt loading on the cathode side can be dramatically reduced to 0.1 mg cm^{-2}, which is much lower than that of the conventional MEA with a Pt loading of 0.25–0.30 mg cm^{-2}; showing the technical advancement of electrospinning. Little effort, however, has been made to decrease the catalyst loading with the MEA of the DMFC by constructing a nanostructured membrane electrode. With the aid of electrospinning, in this work, we report a novel MEA that utilizes a nanofiber network catalytic layer (NNCL) structure in the anode of a passive DMFC. We have found that the formation of 3D NNCL network results in a significant decrease in noble metal loading, while maintaining the similar DMFC's performance in comparison with the conventional MEA.

2. Experimental

2.1. Materials

Polyvinylalcohol (PVA) was purchased from Sigma Aldrich. Nafion solution (5%) was purchased from DuPont Company. PtRu (1:1) black and PtRu (1:1)/C (60 wt. %) as the anode catalysts, Pt black and Pt/C (60 wt. %) as the cathode catalysts were obtained from Johnson Matthey company. Commercial carbon paper (TGPH060, 20 wt. % PTFE, Toray) was obtained from Toray Company. All the chemicals were in an analytical grade.

2.2. Electrospinning construction of the PtRu/C/Nafion/PVA NNCL

Synthesis of PtRu/C/Nafion/PVA nanofibers: An electrospinning ink was prepared by mixing PtRu (1:1) black (Johnson Matthey company) and PtRu (1:1)/C (60 wt. %, Johnson Matthey company) into 5 wt.% Nafion solution (DuPont Company), then adding Polyvinylalcohol (PVA) (MW = 100000 g mol^{-1}, Sigma Aldrich), where the PtRu/C:Nafion:PVA weight ratio was 71/9:14:6. The ink was electrospun at a rate of 0.15 ml h^{-1} by a pump with 15 cm grounded collector to the needle at a high voltage of 16–18 kV.

The conventional membrane electrode assembly (MEA) was prepared as before [23], with a Nafion®115 membrane, a GDE cathode with a Pt loading of 4.0 mg cm^{-2} and a GDE anode with a PtRu loading of 2.0 mg cm^{-2}. The electrospun MEA was prepared with the same membrane and cathode, while the anode was displaced with the nanofiber network catalytic layer with a PtRu loading of 1.0–2.0 mg cm^{-2}.

2.3. Morphology and electrochemical characterization of the nanofiber network

FESEM images were collected on Field Emission Scanning Electron Microscopy (FESEM, Hitachi S-4800) and TEM image was conducted with Field Emission Transmission Electron Microscopy (FETEM, JEOL 2100F).

The cyclic voltammogram (CV) measurement was carried out with Solartron SI1287 Potentiostat/Galvanostat to characterize the electrochemical active surface area (ESA) of the anodes of the MEAs by feeding the water to the anode of a DMFC as the working electrode, humidified H_2 to the cathode at a flow rate of about 5 mL min^{-1} as the counter electrode and reference electrode. The working potential was cycled from 0.05 V to 0.7 V and at a scan rate of 20 mV s^{-1}. Since the ESA calculated by H desorption is only for Pt in the PtRu catalyst, it could be more concise that the ESA is calculated by CO stripping because CO can be adsorbed on the surface of both Pt and Ru in the PtRu catalyst. The CO-stripping voltammogram was performed with Solartron SI1287 Potentiostat/Galvanostat, by feeding the humidified CO pre-adsorbed on the anode as the working electrode, humidified H_2 to the cathode as the counter electrode and reference electrode. The working potential was cycled from 0.05 to 1.0 V and at a scan rate of 20 mV s^{-1}.

The Electrochemical impedance spectra (EIS) of the anodes fabricated by electrospun and GDE methods with a PtRu loading of 2.0 mg cm^{-2} were recorded using a Solartron SI1260 coupled to a Solartron SI1287 Potentiostat/Galvanostat. All the anode impedance spectra recorded were measured between the anode and DHE at the cathode, and the overpotential of the DHE is negligible according to the previous work [38]. Impedance spectra were obtained at a frequency range between 100 kHz and 0.01 Hz at a given potential of 0.40 V/DHE, and the amplitude of the sinusoidal voltage signal is 10 mV.

2.4. The performance evaluation of the passive DMFCs

For a passive DMFC, an MEA is sandwiched between two Au-deposited Ti plates with open areas of ca.75% for both anode and cathode, respectively. On the anode side, there is a methanol reservoir outside Ti plate, methanol is passively diffused into the anodic catalytic layer of an MEA by self-diffusion (i.e., without the use of any pumps). On the cathode side, the MEA is directly exposed onto the ambient atmosphere (i.e., direct use of O_2 from air, so-called "air-breathing" mode). The active cross-sectional area of an

MEA is 2 × 2 cm^2. The polarization curves of the passive DMFCs under air-breathing mode were obtained on an Arbin FET testing system (Arbin Instument Inc., USA) by using 4 M methanol solution. For each discharging current point along the polarization curve, a period of 3 min waiting time was used to obtain the stable voltage. The Faraday efficiency and energy efficiency of an MEA can be calculated from discharging curve at a constant voltage of 0.35 V when the passive DMFC is fed with 5 mL of 4 M methanol solution. The stability of the DMFC was tested at a constant current density of 40 mA cm^{-2} for a period of time with discontinuously feeding with 4 M methanol solution. All the DMFCs' tests were measured at a temperature of 25 ± 1 °C and the humidity of 30%–40% is used for the cathode.

3. Results and discussions

Fig. 1A and B show the field emission scanning electron microscopy (FE-SEM) images of the anodic catalytic layer prepared by conventional GDE method and electrospinning, respectively. As shown in Fig. 1A, the main particle sizes are in the range from tens of nanometer to several micrometers, and the shapes of the particles are irregular. At the same time, the particles in the GDE electrode are stacked compactly, suggesting that the porosity is low. Fig. 1B clearly shows the formation of continuous nanofiber network of the PtRu/C/Nafion/PVA layer. The nanofiber diameter is in the range from 35 to 475 nm with an average fiber diameter of ca.

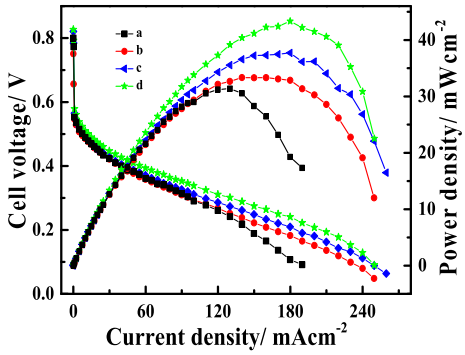

Fig. 2. Polarization curves for four passive DMFCs with the anodic catalytic layers fabricated by a conventional GDE method with a PtRu(1:1) loading of 2.0 mg cm^{-2} (a) and by electrospinning with a PtRu(1:1) loading of 1.0 (b), 1.5 (c) and 2.0 mg cm^{-2} (d). The passive DMFCs were fed with 4mol L^{-1} of CH_3OH at 25 ± 1 °C.

194 nm based on the histogram analysis of 289 nanofibers, as shown in Fig. 1D. Importantly, one can find that the most of PtRu nanoparticles are distributed onto the nanofibers (Fig. 1C). As observed, there is still a slight aggregation of PtRu nanoparticles on the surface of nanofibers since the content of PtRu nanoparticles within the NNCL is as high as 71%. However, such an aggregation of PtRu nanoparticles is much slighter than that of conventional catalytic layer. Furthermore, the nanofibers are stacked loosely while

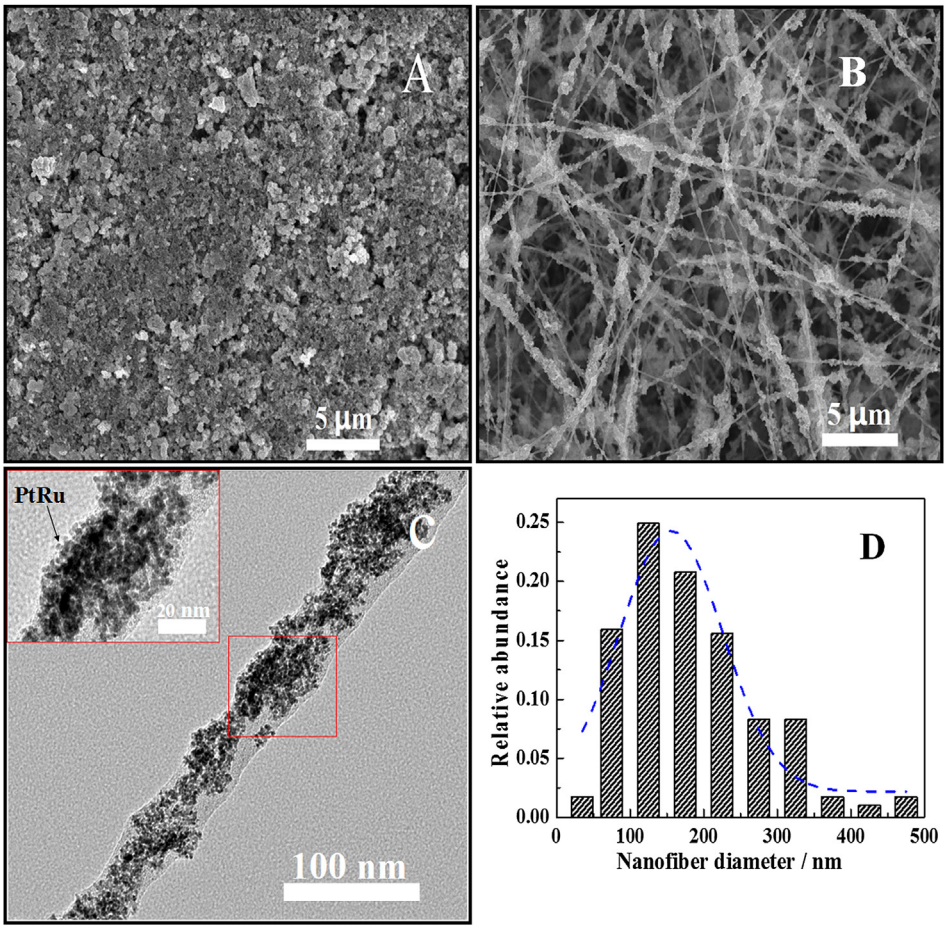

Fig. 1. FESEM images of anodic catalytic layers fabricated by conventional GDE (A) and electrospinning (B) and a typical TEM image (C) of electrospun PtRu–C/Nafion/PVA nanofibers and histogram of the nanofiber diameter distribution for electrospun mat (D).

the porosity is relatively high. The formation of 3D NNCL could facilitate an improvement in both catalyst utilization and mass transportation.

Fig. 2 is a comparison of the polarization curves for the four passive DMFCs with anodic catalytic layers fabricated by conventional GDE and by electrospinning with different PtRu (1:1) loadings. At the same PtRu loading of 2.0 mg cm^{-2}, the maximal power density of the passive DMFC with anodic catalytic layer prepared by electrospinning is 43.0 ± 0.9 mW cm^{-2}, which is much higher than that of the DMFC with GDE anode with a peak power density of 31.3 ± 0.5 mW cm^{-2}. When the PtRu loading within NNCL is decreased to 1.0 mg cm^{-2}, the maximum power density of the DMFC is 33.±1.9 mW cm^{-2}, which is still slightly higher than that by GDE method with a PtRu loading of 2.0 mg cm^{-2}. Obviously, the use of NNCL results in a substantial decrease in PtRu loading but without sacrificing DMFC's performance. Furthermore, at a low current density region, the four passive DMFCs exhibit a similar kinetic and ohmic polarization behavior. However, at a high current density region, a fast decrease in cell's voltage for the MEA fabricated by GDE method is observed in comparison with that of the MEAs by electrospinning, indicating that the mass transportation can be greatly improved for the MEAs with 3D NNCL structure.

To explore the possible reasons for the improved performance of the DMFCs with NNCL, the electrochemical active surface areas of the anodes fabricated by electrospun and GDE methods are calculated. Fig. 3A shows the CVs of the anodes for the four MEAs. The redox peaks in the potential range of 0.05–0.4 V can be attributed to the H adsorption/desorption on the surface of Pt in the PtRu catalyst. The calculated ESAs, as listed in Table 1, by H desorption [39] of the anodes fabricated by GDE method with a PtRu loading of 2.0 mg cm^{-2} and by electrospinning with a PtRu loading of 2.0, 1.5 and 1.0 mg cm^{-2} are ca. 18.0 ± 0.1, 26.7 ± 0.4, 25.6 ± 0.6 and

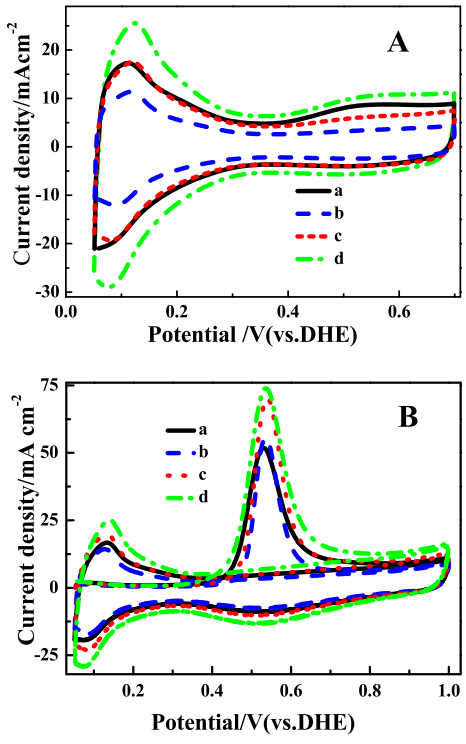

Fig. 3. Cyclic voltammograms (A) and CO-stripping voltammograms (B) of the anodes of four MEAs with the anodic catalytic layers fabricated by a conventional GDE method with a PtRu(1:1) loading of 2.0 mg cm^{-2} (a) and by electrospinning with a PtRu (1:1) loading of 1.0 (b), 1.5 (c) and 2.0 mg cm^{-2} (d).

Table 1
Maximal power density, anodic ESA, Faradic efficiency and energy efficiency of the four passive DMFCs.

Anode loading/ mg cm^{-2}	Maximal power density/ mW cm^{-2}	ESAs by H desorption/ m^2 g^{-1}	ESAs by CO-stripping/ m^2 g^{-1}	Faradic efficiency	Energy efficiency
2.0 (GDE)	31.3 ± 0.5	18.0 ± 0.1	33.7 ± 0.6	44.1%	13.1%
1.0 (Electrospinning)	33.0 ± 1.9	25.3 ± 0.7	52.5 ± 0.4	53.6%	15.9%
1.5 (Electrospinning)	37.9 ± 1.4	25.6 ± 0.6	51.1 ± 0.8	54.5%	16.2%
2.0 (Electrospinning)	43.0 ± 0.9	26.7 ± 0.4	50.5 ± 1.4	65.9%	20.6%

The DMFCs were tested at 25 ± 1 °C under ambient pressure.

25.3 ± 0.7 m^2 g^{-1}, respectively; indicative of a significant improvement in catalyst utilization of the anodic catalytic layer fabricated by electrospinning. The CO stripping voltammograms of the different anodic catalytic layers are shown in Fig. 3B and the calculated ESAs by CO stripping [40] are also listed in Table 1. The calculated ESAs by CO stripping for the GDE anode with a PtRu loading of 2.0 mg cm^{-2} and for the electrospun anodes with a PtRu loading of 2.0, 1.5 and 1.0 mg cm^{-2} are ca. 33.7 ± 0.6, 50.5 ± 1.4, 51.1 ± 0.8 and 52.5 ± 0.4 m^2 g^{-1}, respectively; showing an increase of ~55% in ESA. Normally, the ESAs would reduce with increased PtRu loading because of aggregation. However, the electrospun catalytic layers with different PtRu loadings have nearly similar ESA values, strongly suggesting that the ratio of PtRu nanoparticles distributed on the surface of nanofibers is close to each other even at different PtRu loadings, and thus confirming that the formation of nanofiber network prevents PtRu nanoparticles from aggregation.

Further impedance analysis indicates that the charge transfer resistance of the MEA prepared by electrospinning is smaller than that by GDE method. Overall, the enhanced performance of the DMFCs with the anodic catalytic layers fabricated by electrospinning is ascribed to increase in catalyst utilization and decrease in charge transfer resistance.

To explore the effects of anodic catalytic layers on methanol transfer, Fig. 4 shows the discharging curves of four passive DMFCs with anodic catalytic layers fabricated by electrospinning and conventional GDE methods. For the passive DMFCs with the anodic catalytic layer fabricated by GDE method with a PtRu loading of 2.0 mg cm^{-2} and by electrospinning with PtRu loadings of 1.0 and 1.5 mg cm^{-2}, the discharge curves can be divided into three regions. At the early stage, the discharge current decreases within ca. 20 min. Then, the current slightly increases with time for a period of time. The slight increase in current might be attributed to an increase in cell temperature caused by methanol crossover and to an efficient transport of methanol from the reservoir to the anode catalyst layer. After discharging for ca. 2 h, the current starts to continuously decrease as the methanol concentration in the reservoir decreases. For the passive DMFC with the NNCL with a PtRu loading of 2.0 mg cm^{-2}, the discharge current continuously decays with time, probably due to the fact that the rate of methanol transfer from the reservoir to the anode catalyst layer is lower than that of methanol consumed on the catalytic layer since the peak power density of this DMFC as shown in Fig. 2 is the highest. For the four passive DMFCs, both Faradic efficiency and energy efficiency are calculated and shown in Table 1. The energy efficiency of the anodes fabricated by GDE method with a PtRu loading of 2.0 mg cm^{-2} and by electrospinning with a PtRu loading of 2.0, 1.5 and 1.0 mg cm^{-2} are ca. 13.1%, 15.9%, 16.2% and 20.6%, respectively. Clearly, the energy efficiency was improved greatly when using the NNCLs. The insert in Fig. 4 demonstrates a 120 h durability test of a passive DMFC with electrospun NNCL with a PtRu loading of 2.0 mg cm^{-2}. Clearly, the

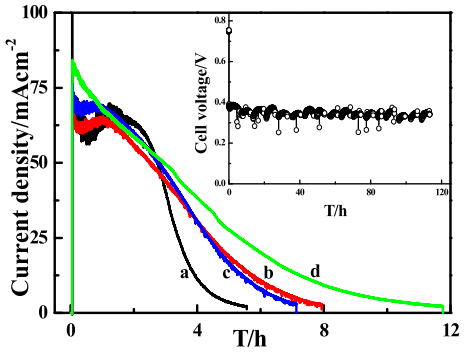

Fig. 4. Transient discharge curves of the passive DMFCs with the anodic catalytic layers fabricated by a conventional GDE method with a PtRu (1:1) loading of 2.0 mg cm^{-2} (a) and by electrospinning with a PtRu (1:1) loading of 1.0 (b), 1.5 (c), and 2.0 mg cm^{-2} (d), respectively. The discharge was conducted at a constant voltage of 0.35 V for the DMFCs fed with 5 mL of 4 mol L^{-1} methanol. Insert: the stability of a DMFC with electrospun catalytic layer of 2.0 mg cm^{-2} PtRu and at a constant current of 40 mA cm^{-2}.

discharging voltage keeps at ca. 0.35 V with some fluctuation at a given current density of 40 mA cm^{-2}, confirming that the stability of such a DMFC is quite good for the practical application with an improved cell performance. The voltage fluctuation may be due to the water flooding at cathode side and to the possible change in methanol concentration during the test.

Fig. 5A presents EIS spectra of the anodes of the MEAs and an equivalent circuit model as shown in Fig. 5B. In this model, the constant phase elements (CPE) are used to replace ideal capacitors, which are commonly found in conventional equivalent circuit models, to account for the non-uniform structure of the related electrode section [41]. Thus, the physical meanings of each element employed in the equivalent circuit model (Fig. 5B) are as follows:

R_m is the resistance of the membrane;

The anode-membrane interface contribution contains CPE_i and R_i, describing the capacitive behavior and contact resistance between the membrane and the catalyst layer, respectively;

R_{ct} is the charge transfer resistance;

CPE_{dl} describes the capacitive behavior of the real anode with roughness of the catalyst layer and non-uniform catalyst distribution;

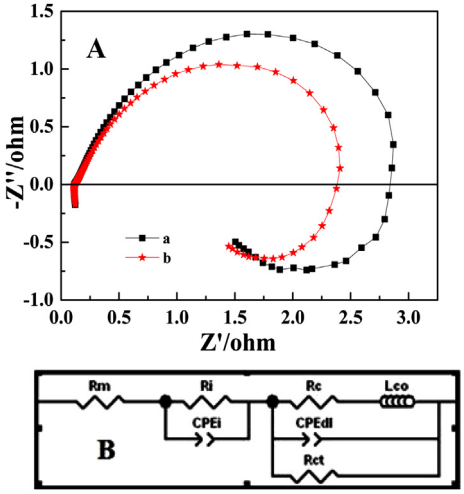

Fig. 5. Electrochemical impedance spectra (A) and equivalent circuit (B) of the anodes of the two MEAs with the anodic catalytic layers fabricated by conventional GDE (a) and electrospinning (b) with a PtRu(1:1) loading of 2.0 mg cm^{-2} at a given DC potential of 0.4 V/DHE.

Table 2
Fitted parameters for the CPE-based equivalent circuit model for the anode of the passive DMFCs operating at 0.4 V/DHE and at 25 ± 1 °C.

Parameter	2.0 mg cm^{-2} (GDE)	2.0 mg cm^{-2} (Electrospinning)
R_m (Ohm cm^2)	0.126	0.127
R_i (Ohm cm^2)	0.051	0.068
CPE_i-T (F cm^{-2})	0.374	0.314
CPE_i-P	0.990	0.927
R_c (Ohm cm^2)	2.989	2.373
L_{co} (H cm^{-2})	19.85	17.00
CPE_{dl}-T (F cm^{-2})	0.344	0.508
CPE_{dl}-P	0.895	0.906
R_{ct} (Ohm cm^2)	1.644	1.328

L_{co} means that the current signal follows voltage perturbation with a phase-delay due to slowness of CO desorption;

R_c is the resistance of the solid phase in anodic catalytic layer.

The fitted parameters are provided in Table 2. As observed, the values of R_c, L_{co} and R_{ct} of the anodic catalytic layer fabricated by electrospinning are smaller than that with conventional GDE, which can explain the improved performance of the DMFC using NNCL as shown in Figs. 2 and 4.

4. Conclusions

In conclusion, the construction of anodic catalytic layer with a nanofiber 3D network structure leads to a significant increase in catalyst utilization and a decrease in charge transfer resistance of the DMFCs, thus greatly enhancing the DMFC's performance and allowing a dramatic reduction in noble metal loading within the membrane electrode assembly. The formation of nanofiber 3D network structure could be responsible for the improved performance.

Acknowledgments

We would like to thank the National Basic Research Program of China (973 Program, 2012CB932800), the Nature Science Foundation of China (21373256), Shanghai Science and Technology Committee (11DZ1200400, 12ZR1431200) and the Knowledge Innovation Engineering of the Chinese Academy of Sciences (12406, 124091231) for support to this work.

References

[1] A.S. Aricò, S. Srinivasan, V. Antonucci, Fuel Cells 1 (2001) 133–161.
[2] M. Winter, R.J. Brodd, Chem. Rev. 101 (2004) 4245–4270.
[3] H. Joh, S. Hwang, J. Cho, T. Ha, S. Kim, S. Moon, H. Ha, Int. J. Hydrogen Energy 33 (2008) 7153–7162.
[4] M.Y. Li, S.Z. Zhao, G.Y. Han, B.S. Yang, J. Power Sources 191 (2009) 351–356.
[5] A. Morozan, B. Jousselme, S. Palacin, Energy Environ. Sci. 4 (2011) 1238–1254.
[6] X.G. Wang, J.H. Liao, C.P. Liu, W. Xing, T.H. Lu, Electrochem. Commun. 11 (2009) 198–201.
[7] H. Yang, Angew. Chem. Int. Ed. 50 (2011) 2674–2676.
[8] J.X. Wang, H. Inada, L. Wu, Y. Zhu, Y. Choi, P. Liu, W.P. Zhou, R.R. Adzic, J. Am. Chem. Soc. 131 (2009) 17298–17302.
[9] Z.D. Wei, L.L. Li, Y.H. Luo, C. Yan, C.X. Sun, G.Z. Yin, P.K. Shen, J. Phys. Chem. B 110 (2006) 26055–26061.
[10] Z.Y. Bai, L. Yang, L. Li, J. Lv, K. Wang, J. Zhang, J. Phys. Chem. C. 113 (2009) 10568–10573.
[11] E. HaoYu, S. Cheng, K. Scott, B. Logan, J. Power Sources 171 (2007) 275–281.
[12] D.H. Lee, W.J. Lee, W.J. Lee, S.O. Kim, Y.H. Kim, Phys. Rev. Lett. 106 (2011) 175502.
[13] Y.S. Kim, S.H. Nam, H.S. Shim, H.J. Ahn, M. Anand, W.B. Kim, Electrochem. Commun. 10 (2008) 1016–1019.
[14] J.Y. Cao, C. Du, S.C. Wang, P. Mercier, X.G. Zhang, H. Yang, D.L. Akins, Electrochem. Commun. 9 (2007) 735–740.
[15] C.A. Bessel, K. Laubernds, N.M. Rodriguez, R.T.K. Baker, J. Phys. Chem. B 105 (2001) 1115–1118.
[16] M.S. Wilson, S. Gottesfeld, J. Appl. Electrochem. 22 (1992) 1–7.
[17] M.S. Wilson, J.A. Valerio, S. Gottesfeld, Electrochim. Acta 40 (1995) 355–363.

[18] Y.G. Chun, C.S. Kim, D.H. Peck, D.R. Shin, J. Power Sources 71 (1998) 174–178.
[19] H. Tang, S. Wang, M. Pan, S.P. Jiang, Y. Ruan, Electrochim. Acta 52 (2007) 3714–3718.
[20] S.L. Wang, G.Q. Sun, G.X. Wang, Z.H. Zhou, X.S. Zhao, H. Sun, X.Y. Fan, B.L. Yi, Q. Xin, Electrochem. Commun. 7 (2005) 1007–1012.
[21] Q. Mao, G.Q. Sun, S.L. Wang, H. Sun, G.X. Wang, Y. Gao, A.W. Ye, Y. Tian, Q. Xin, Electrochim. Acta 52 (2007) 6763–6770.
[22] M. Michel, A. Taylor, R. Sekol, P. Podsiadlo, P. Ho, N. Kotov, L. Thompson, Adv. Mater. 19 (2007) 3859–3864.
[23] T. Yuan, Y.Y. Kang, J. Chen, C. Du, Y.J. Qiao, X.Z. Xue, Z.Q. Zou, H. Yang, Int. J. Hydrogen Energy 36 (2011) 10000–10005.
[24] M.K. Debe, A.K. Schmoeckel, G.D. Vernstrom, R. Atanasoski, J. Power Sources 161 (2006) 1002–1011.
[25] S. Ramakrishna, K. Fujihara, W.E. Teo, T. Yong, Z. Ma, R. Ramaseshan, Mater. Today 9 (2006) 40–50.
[26] A. Greiner, J.H. Wendorff, Angew. Chem. Int. Ed. 46 (2007) 5670–5703.
[27] X. Li, G. Cheruvally, J.K. Kim, J.W. Choi, J.H. Ahn, K.W. Kim, H.J. Ahn, J. Power Sources 167 (2007) 491–498.
[28] J.R. Kim, S.W. Choi, S.M. Jo, W.S. Lee, B.C. Kim, Electrochim. Acta 50 (2004) 69–75.
[29] B.H. Kim, K.S. Yang, H.G. Woo, Electrochem. Commun. 13 (2011) 1042–1046.
[30] A. Laforgue, J. Power Sources 196 (2011) 559–564.
[31] S. Marx, M.V. Jose, J.D. Andersen, A.J. Russell, Biosens. Bioelectron. 26 (2011) 2981–2986.
[32] A. Stafiniak, B. Boratyński, A. Baranowska-Korczyc, A. Szyszka, M. Ramiączek-Krasowska, J. Prażmowska, K. Fronc, D. Elbaum, R. Paszkiewicz, M. Tłaczała, Sens. Actuators, B 160 (2011) 1413–1418.
[33] B. Guo, S.Z. Zhao, G.Y. Han, L.W. Zhang, Electrochim. Acta 53 (2008) 5174–5179.
[34] X.M. Liu, M.Y. Li, G.Y. Han, J.H. Dong, Electrochim. Acta 55 (2010) 2983–2990.
[35] W. Zhang, P.N. Pintauro, ChemSusChem 4 (2011) 1753–1757.
[36] X.L. Wang, H.M. Zhang, J.L. Zhang, H.F. Xu, X.B. Zhu, J. Chen, B.L. Yi, J. Power Sources 162 (2006) 474–479.
[37] H.F. Oetjen, J. Electrochem. Soc. 143 (1996) 3838–3842.
[38] K.T. Jeng, C.C. Chien, N.Y. Hsu, W.M. Huang, S.D. Chiou, S.H. Lin, J. Power Sources 164 (2007) 33–41.
[39] M.J. Ren, J. Chen, Y. Li, H.F. Zhang, Z.Q. Zou, X.M. Li, H. Yang, J. Power Sources 246 (2014) 32–38.
[40] W. He, J.Y. Liu, Y.J. Qiao, Z.Q. Zou, X.G. Zhang, D.L. Akins, H. Yang, J. Power Sources 195 (2010) 1046–1050.
[41] N.Y. Hsu, S.C. Yen, K.T. Jeng, C.C. Chien, J. Power Sources 142 (2005) 169–176.